ROLE OF ISOVECTOR-ISOSCALAR COUPLING ON CHARGE RADIUS OF HEAVY AND SUPERHEAVY NUCLEI

Netta Liliani*

Teknik Mesin, Fakultas Teknik, Universitas Islam 45, Bekasi 17113, Indonesia

*Corresponding Author Email: netta.liliani@gmail.com

ABSTRACT

We have investigated the effect of the isovector-isoscalar coupling on the finite nuclei and nuclear matter properties, the neutron skin thickness of ^{208}Pb, and the charge radius on heavy and superheavy nuclei calculated by the relativistic mean-field (RMF) model. In this work, we generates two parameter sets, i.e., PTE16 and PTE31. The numbers 16 and 31 denote the isovector-isoscalar coupling terms, while T and E denote the tensor coupling and electromagnetic exchange terms, respectively. We found that PTE16 and PTE31 are compatible with the constraints obtained by R. Essick, *et al.*, arXiv: 2102.10074v1 [nucl-th] (2021). We also found that the increase of the isovector-isoscalar coupling terms gives a significant effect on the binding energy and the charge radius on heavy nuclei except for the charge radius of ^{208}Pb. Increased of the isovector-isoscalar coupling terms make the values of charge radius prediction increase too, but vice versa for the neutron skin thickness and nuclear matter prediction. PTE31 yields symmetry energy $J = 31.521$ MeV, slope $L = 57.643$ MeV, and neutron skin thickness $= 0.21419$ fm. While the β_2 correction (for deform nuclei) does not always give a significant effect on the charge radius.

Keywords: isovector-isoscalar coupling, charge radius, heavy nuclei, superheavy nuclei

INTRODUCTION

The nuclear charge radius along the isotope chains became a hot topic in recent discussion. It's being one of the most fundamental properties of a nucleus, plays vital role in our understanding of complex dynamics of atomic nuclei [1]. The knowledge of nuclear size plays an important role not only in understanding new physics beyond standard model (SM) but also serving as input quantities in astrophysical study [2]. Nuclear charge radius is a key observable that can directly reflect the important characteristics on the nuclear structure. For instance, nuclear charge radius could give signals for the occurrence of new magic number or the disappearance of traditional magic number considering the influence of shell effect on charge radii [3]. But, the research on charge radii of superheavy nuclei (SHN) is sort of beyond the ability of available experimental tools due to the quite short lifetimes [2].

In the beginning, the nuclear charge radius R_0 is usually described by the $A^{1/3}$ law: $R_0 = r_0 A^{1/3}$, where A is the mass number [3]. The root-mean-square (rms) nuclear charge radius can be self-consistently calculated by using microscopic nuclear mass models, such as the relativistic mean field (RMF) model [3]. The mean field theory makes a considerable success in describing the fundamental properties of finite nuclei and nuclear matter [4]. The rms charge radius can be calculated from the following formula:

$$r_c\left(A\right) = \sqrt{\left\langle r^2 \right\rangle^A} = \sqrt{\left\langle r^2 \right\rangle^{A'} + \delta \left\langle r^2 \right\rangle^{A'A}} \tag{1}$$

where A' represents the mass number of stable reference isotope.

The other fundamental physical observable is neutron skin thickness Δr_{np}, is defined by the difference between the neutron and proton root-mean-square radius, are indispensable in nuclear reaction and nuclear astrophysics research [5]. Δr_{np} predicted by proton elastic scattering is a relatively narrower range of ^{208}Pb skin, i.e., $\Delta r_{np} = 0.148\text{-}0.265$ fm [6]. Furthermore, the elastic scattering of polarized electrons from ^{208}Pb, known as the ^{208}Pb Radius Experiment (PREX) at the Jefferson Lab, has provided the first model-independent evidence in favor of a neutron-rich skin with $\Delta r_{np} = 0.15\text{-}0.49$ fm [7.8]. The accuracy has been improved in the upgraded second stage experiment Δr_{np} of ^{208}Pb (PREX-II) $= 0.212\text{-}0.354$ fm [9]. Combining astrophysical data with PREX-II and chiral effective field theory yields $J = 34 \pm 3$ MeV and $L = 58 \pm 19$ MeV [10].

Motivated by the finding of the author's previous work [5,11] that the tensor couplings, Coulomb exchange $C_{\text{EXC}}^{\text{EM}}$ and isovector-isoscalar coupling $\eta_{2\rho}$ terms in the RMF model have an impact on the neutron skin thickness of nuclei prediction, a peculiarity of significantly thick skin thickness of ^{208}Pb [12]. In this work, we will investigate the minimum and maximum values of isovector-isoscalar coupling that are compatible with the constraints in Ref. [10], and also investigate the effect of isovector-isoscalar coupling not only on the neutron skin thickness of ^{208}Pb but also on the finite nuclei and nuclear matter properties, as well as charge radius on heavy and superheavy nuclei with the β_2 correction for deformed nuclei. In this work, we used the constraints in Ref. [10] that were published in arXiv but the difference is

not much from a newly published article. For suggestion, the constraints in a newly published article can be the next research.

We organize this work as follows. Section II presents the method (formalism of RMF model), Sec. III presents the result and discussions. The conclusion is given in Sec. IV

METHOD

In this section we briefly review the formalism of the RMF model with additional tensor couplings, the coulomb exchange and the various isovector-isoscalar couplings, with the equations and the step of fitting in Ref. [5,11]. The Lagrangian density of the RMF model is:

$$L_{\text{RMF}} = L_{\text{N}} + L_{\text{M}} + L_{\text{LIN}} + L_{\text{NONLIN}} + L_{\text{T}} + L_{\rho\omega} + L_{\text{EXC}}^{\text{EM}} \tag{2}$$

With

$$L_{\text{N}} = \sum_{j=1}^{A} \bar{\psi}_j \left[i\gamma^\mu \partial_\mu - M \right] \psi_j \tag{3}$$

$$L_{\text{M}} = \frac{1}{2}\left(\partial_\mu \phi \partial^\mu \phi - m_\sigma^2 \phi^2\right) - \frac{1}{2}\left(\frac{1}{2}V_{\mu\nu}V^{\mu\nu} - m_\omega^2 V_\mu V^\mu\right) - \frac{1}{2}\left(\frac{1}{2}R_{\mu\nu}R^{\mu\nu} - m_\rho^2 R_\mu R^\mu\right) - \frac{1}{2}\partial^\nu A^\mu \partial_\nu A_\mu \tag{4}$$

$$L_{\text{LIN}} = \sum_{j=1}^{A} \bar{\psi}_j \left(g_\sigma \phi - g_\omega \gamma^\mu V_\mu - \frac{1}{2}g_\rho \gamma^\mu \tau R_\mu - eA^\mu \frac{1+\tau_0}{2}\gamma_\mu \right)\psi_J \tag{5}$$

$$L_{\text{NONLIN}} = -\left(\frac{k_3}{6M}g_\sigma m_\sigma^2 \phi^3 + \frac{k_4}{24M^2}g_\sigma^2 m_\sigma^2 \phi^4\right) + \frac{1}{24}\xi_0 g_\omega^2 \left(V_\mu V^\mu\right)^2 \tag{6}$$

$$L_{\text{T}} = -\sum_{j=1}^{A}\left(\frac{f_\omega}{2M}\partial^\nu V^\mu \bar{\psi}_j i\gamma_\mu \gamma_\nu \psi_j + \frac{f_\rho}{4M}\partial^\nu R^\mu \bar{\psi}_j \tau i\gamma_\mu \gamma_\nu \psi_j\right) \tag{7}$$

$$L_{\rho\omega} = \frac{\eta_{2\rho}}{4M^2}g_\omega^2 m_\rho^2 V_\mu V^\mu R_\mu R^\mu \tag{8}$$

$$L_{\text{EXC}}^{\text{EM}} = C_{\text{EXC}}^{\text{EM}}\left[\frac{3}{4}e^2\left(\frac{3}{\pi}\right)^{\frac{1}{3}}\right]\rho_p^{\frac{4}{3}}\left[1 - \frac{1}{3M^2}\left(3\pi^2\right)^{\frac{2}{3}}\rho_p^{\frac{2}{3}}\right] \tag{9}$$

Where, L_{N} is free nucleon Lagrangian written in the Dirac equation. ψ and M are nucleon field and mass. L_{M} is free meson Lagrangian written in the Klein Gordon equation [13]. m_σ is the mass of scalar-isoscalar (σ), m_ω is the mass of vector-isoscalar (ω), m_ρ is the mass of vector-isovector (ρ). ϕ, V_μ and R_μ are the meson fields of σ, ω, and ρ mesons, respectively. A_μ is a photon field. L_{LIN} is the linear meson-nucleon Lagrangian which is described interaction between nucleon and meson, as well as nucleon and photon. g_σ, g_ω, g_ρ are the coupling constants of σ, ω, and ρ mesons, respectively. L_{NONLIN} is the nonlinear meson-nucleon Lagrangian which is described meson interaction in high density. L_{T} is the tensor Lagrangian. Where f_ω and f_ρ are isoscalar and isovector tensor coupling constants,

respectively. $L_{\rho\omega}$ is the cross interaction isovector-isoscalar-vector term, here $\eta_{2\rho}$ is the isovector-isoscalar coupling term. The last, L_{EXC}^{EM} is the relativistic Local-Density Approximations (LDA) form of the Coulomb exchange energy density. Those lagrangian equations were derived to get energy density equations that are input in the fitting process.

RESULT AND DISCUSSION

Parametrization

The value of each parameter set was obtained by a fitting process with the experimental data of finite nuclei observables [3], using a similar fitting protocol used in Refs. [5,11]. Here, we used the experimental data of the 14 nuclei binding energies and 13 nuclei charge radius of, and also used parameterization weight in order of 0.15% and 0.3% for the binding energies and charge radius, respectively. The nuclei experimental data were taken from the isotope and isotone chains of light, medium, and heavy nuclei [3]. The $\eta_{2\rho}$ and C_{EXC}^{EM} were not included in the fitting process. The C_{EXC}^{EM} set as 1, meanwhile, the constant of $\eta_{2\rho}$ values must be searched in order to be compatible with the maximum and the minimum constraint in Ref. [10]. After passing the fitting process, we found $\eta_{2\rho} = 0.016$ and $\eta_{2\rho} = 0.031$ for the maximum and minimum constraints, respectively. The parameter values which was obtained by the fitting process are shown in TABLE 1

TABLE 1. Parameter values of each parameter set

	PTE16	PTE31
m_σ	479.5635	479.5914
g_σ	9.769872	9.769446
g_ω	13.03916	13.03901
g_ρ	4.906256	5.512283
c_1	164.4657	164.5762
b_3	6.399211	6.251837
b_2	−7.770342	−7.783044
f_ω	−0.2417256	−0.2492481
f_ρ	2.641816	2.900979
C_{EXC}^{EM}	1	1
$\eta_{2\rho}$	0.016	0.031

The difference in the value of each parameter set is not significant, this is due to the difference of $\eta_{2\rho}$ which is not too far away. The most obvious difference from the table above is that g_ρ and f_ρ are comparable to $\eta_{2\rho}$. Although the difference values of each parameter set are not significant, these results will be more clearly shown in the next figures and the tables of nuclear matter properties.

Finite Nuclei Properties

To see the performance of the parameter sets used in this work, we can check the accuracy of the parameter sets through the percentage of the relative error of each parameter set shown in FIGURE 1, with compared experimental data in Ref. [3].
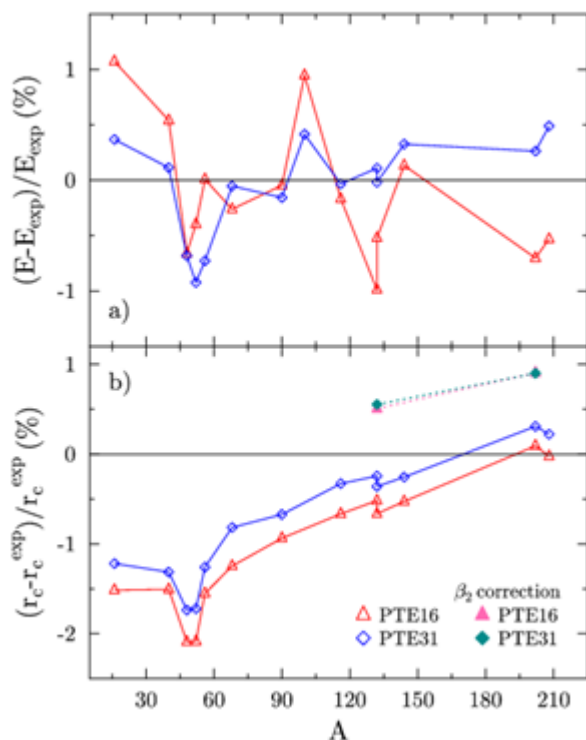
FIGURE 1. Percentage of the relative error to the (a) binding energy and (b) charge radius as a function of mass number A with β_2 correction as predicted by the 2 parameter sets as a function of mass number for light, medium, and heavy nuclei.

The percentage of relative error, i.e., the difference between calculation and experimental values divided by the experimental value in %, can be used as the media to observe the performance or global quality of a parameter set outside its fitting window because this observable is quite sensitive to the differences between parameter-set predictions used [11]. The percentage of relative error could have positive and negative values. Positive values show the prediction of parameter sets greater than the experiment data, and conversely. The prediction will get better when it approaches or is on the zero line. Based on Fig. 1, the relative error of each parameter set is approximately between -1.0 - 1.0 % for binding energy (panel a) and -2.1 - 0.3 % for charge radius (panel b). The increase of the $\eta_{2\rho}$ value gives a significant effect on the binding energy and the charge radius prediction. It gives an attractive effect, so it can be closer to experimental data. But, the charge radius prediction on ^{208}Pb is better when the value $\eta_{2\rho}$ decreased.

The charge radius for the deformed nuclei needs corrections. In our observable, there are two deformed nuclei we used, i.e., $Xe\left(A=132\right)$ and $Hg\left(A=202\right)$. Considering the isospin and shell

effects in the nucleus, a four-parameter nuclear charge radii formula was proposed by combining the shell corrections and deformations of nuclei obtained from the Weizsacker-skyrme mass model [3]. The formula is expressed as:

$$r_c = r_c^{\text{spherical}} \left(1 + \frac{8}{5\pi} (\beta_2)^2 \right)$$

(10)

Where β_2 represents the quadrupole deformation of the nucleus (we can check the β_2 value in Ref. [14]). However, looking at FIGURE 1b above, the charge radius prediction with the β_2 correction actually moved away from the experimental data. In other words, the β_2 correction does not always give a significant effect, in this work it gives a repulsive effect, so it decreases the predictions.

Nuclear Matter Properties

The most precisely determined of symmetric nuclear-matter properties is binding energy at saturation density (E). At saturation density $\rho = \rho_0$, general pressure $P \approx 0$, and binding energy $E \approx -16$ MeV [11], other nuclear matter properties at the saturation density can be derived from the binding energy $E(\rho)$:

$$K = 9\rho_0^2 \frac{d^2 E(\rho)}{d\rho^2} \bigg|_{\rho=\rho_0}$$

(11)

$$J = 27\rho_0^3 \frac{d^3 E(\rho)}{d\rho^3} \bigg|_{\rho=\rho_0}$$

(12)

where, K and J are Incompressibility and its corresponding slope, respectively. While in the isovector sector, the role of $E(\rho)$ replaced by $J(\rho)$, they are L, K_{sym}, K_{asy}, and K_{sat2}:

$$L = 3\rho_0 \frac{dJ(\rho)}{d\rho} \bigg|_{\rho=\rho_0}$$

(13)

$$K_{\text{sym}} = 9\rho_0^2 \frac{d^2 J(\rho)^2}{d\rho} \bigg|_{\rho=\rho_0}$$

(14)

$$K_{\text{asy}} = K_{\text{sym}} - 6L$$

(15)

$$K_{\text{sat2}} = K_{\text{asy}} - \frac{J_0}{K_0} L$$

(16)

the constraints that we adopted in this work i.e., $J = 31-37$ MeV, $L = 39-77$ MeV, and $\Delta r_{\text{np}} = 0.212 - 0.354$ fm. The effect of $\eta_{2\rho}$ in nuclear matter properties are shown in TABLE 2.

TABLE 2. Nuclear matter properties predicted by 2 parameter sets

	PTE16	PTE31
$E\,(\mathrm{MeV})$	–15.909	–15.906
$K\,(\mathrm{MeV})$	219.277	221.441
$J\,(\mathrm{MeV})$	33.136	31.521
$L\,(\mathrm{MeV})$	75.117	57.643
$K_{\mathrm{sym}}\,(\mathrm{MeV})$	–76.957	–54.778
$K_{\mathrm{asy}}\,(\mathrm{MeV})$	–527.660	–400.639
$K_{\mathrm{sat2}}\,(\mathrm{MeV})$	–377.818	–288.136

From the table above, all values in the parameter sets will decrease with increased the $\eta_{2\rho}$ value, except for the incompressibility K. At first glance we think, the value in PTE16 can be minimized until reaches the maximum constraint, but in our previous work [5], slope L from PTE15 has reached 77.574 MeV. So, PTE16 and PTE31 have reached the maximum and minimum values of the constraints above. The neutron skin thickness from the fitting process of PTE16 and PTE31 i.e., 0.24874 fm and 0.21419 fm, respectively. The role of the isovector-isoscalar coupling term on nuclear matter properties and neutron skin thickness are similar, i.e., increased of the $\eta_{2\rho}$ value making the prediction values decrease.
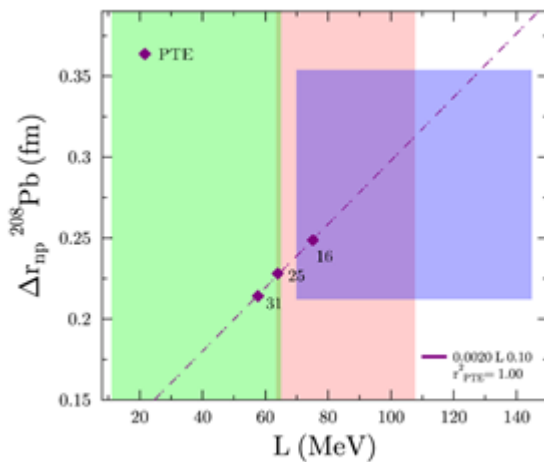
FIGURE 2. Neutron skin thickness Δr_{np} as predicted by the 2 parameter sets as a function of L. We compare the present result with the range for L deduced from GW170817 [15] in light-green, light-red colour from Ref. [16]. and Shaded purple region are the implications of the PREX-II from Ref. [17]. The number 16, 25, and 31 denote the isovector-isoscalar coupling values.

Δr_{np} of ^{208}Pb a quantity strongly correlated with slope L [10]. Their correlation can be investigated in FIGURE 2. Based on Figure above, parameter sets with the larger isovector-isoscalar coupling value compatible with constraint in Ref [15], and vice versa, parameter set with the smaller isovector-isoscalar coupling value compatible with constraint PREX-II [17].

The Nuclear Charge Radius for Heavy and Superheavy Nuclei

In this section, we investigate the isovector-isoscalar coupling's effect on the charge radius of heavy nuclei isotopes (see FIGURE 3) with β_2 correction for deformed nuclei and compared the present result with the experimental data in Ref. [3]. The bottom panel shows the percentage of relative error for each parameter. Based on FIGURE. 3a, the charge radius of $_{82}$Pb isotopes predicted by PTE16 is closer to the experimental data with a relative error between -0.12 – 0.08%. Conversely, PTE16 makes the charge radius prediction of $_{86}$Rn and $_{88}$Ra isotopes far away from the experimental data, with a maximum relative error is 0.5% and 0.7%, respectively. So, we can conclude that the role of isovector-isoscalar coupling is differ, depending on the nuclei. Nevertheless, the relative error from both parameter sets is less than 1 %, in another word those parameter sets are still compatible to investigate the charge radius. The decrease of the $\eta_{2\rho}$ value gives an attractive effect on the charge radius of $_{82}$Pb isotopes and gives a repulsive effect on $_{86}$Rn and $_{88}$Ra isotopes. While the β_2 correction only gives a significant effect on the charge radius of $_{86}$Rn isotopes.

In the last investigation, we completed the prediction of charge radius for SHN, i.e., ^{292}120 isotopes, predicted by two-parameter sets that are shown in FIGURE 4. The research on charge radii of SHN is sort of beyond the ability of available experimental tools due to the quite short lifetimes [2]. A mass number of nuclei and charge radius have a linear relationship, where the increase of mass number will be accompanied by the increase of charge radius. The magnitude of charge radius for heavy nuclei < 6 fm and for superheavy nuclei > 6 fm. Based on FIGURE 4, the increase of the $\eta_{2\rho}$ value makes the prediction of charge radius increase, too.
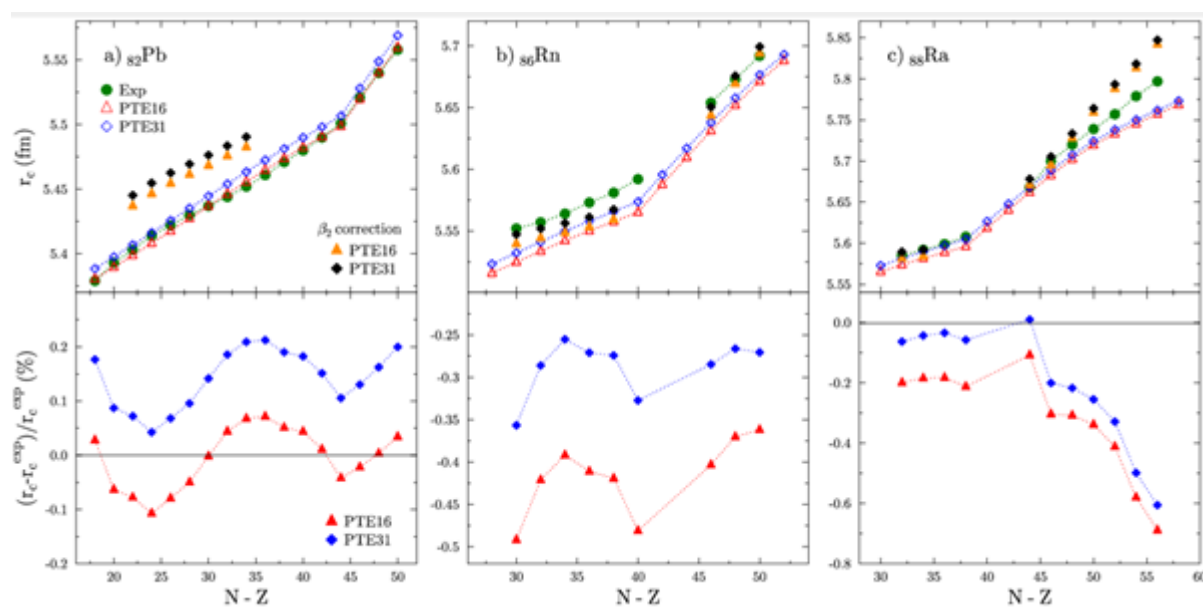
FIGURE 3. Top panel show the charge radius r_c of a). $_{82}$Pb, b). $_{86}$Rn, c). $_{88}$Ra isotopes with the β_2 correction, and bottom panel show the percentage of relative error as a function of N – Z predicted by 2 parameter sets. We compare the present result with the experimental data in Ref. [3].
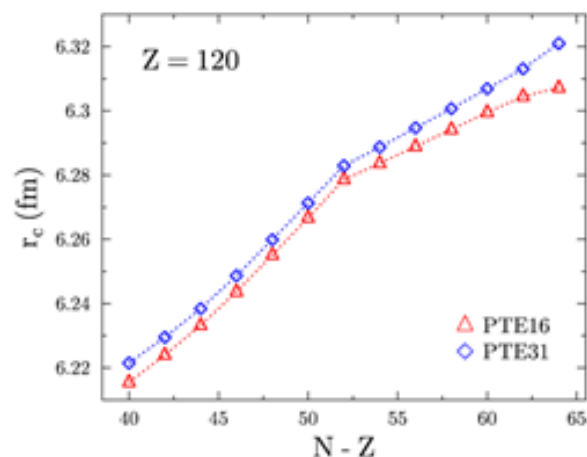
FIGURE 4. The charge radius prediction of Z = 120 isotopes as a function of N – Z predicted by 2 parameter sets.

CONCLUSION

In conclusion, we has systematically investigated the influence of isovector-isoscalar coupling. We adopted the constraints used in this work, i.e., $J = 31 - 37$ MeV , $L = 39 - 77$ MeV and $\Delta r_{np} = 0.212 - 0.354$ fm , so the parameters set that compatible with those constraints are PTE16 and PTE31. The increase of the $\eta_{2\rho}$ value gives an attractive effect on the binding energy and the charge radius prediction, so it can be closer to the experimental data, but not for the charge radius prediction on ^{208}Pb, it's better when the value $\eta_{2\rho}$ decreases. While, the charge radius prediction on other heavy nuclei, such as in $_{86}$Rn and $_{88}$Ra isotopes will better when the value $\eta_{2\rho}$ increases. The β_2 correction is only give a significant effect in the charge radius of $_{86}$Rn isotopes. The charge radius prediction for SHN (^{292}120) yields the influence that the increase of the $\eta_{2\rho}$ value makes the prediction increase, too. The last, on the nuclear matter properties, all values in the parameter sets will decrease with increase the $\eta_{2\rho}$ value. So, it will be very influential on neutron skin thickness.

REFERENCES

[1]   X. X. Dong *et al*., "Novel Bayesian neural network based approach for nuclear charge radii," Physical Review C, vol. 105, p. 014308, 2022.

[2]   R. An *et al*., "Systematic study of nuclear charge radii along Z = 98-120 isotopic chains," *arXiv preprint*, vol. 2112, p. 03829, 2021.

[3]   T. Li *et.al*., "Compilation of recent Nuclear Ground State Charge Radius Measurements and Test for Models," *Atomic Data and Nuclear Data Tables,* vol. 140, p. 101440, 2021.

[4]   J. Meng, P. Ring and P. W. Zou, "in Relativistic Density Functional for Nuclear Structure (International Review of Nuclear Physics-Vol 10)," *edited by J. Meng (World Scientific*, Singapore, 2016.

[5]   N. Liliani *et al*., "Tensors and Coulomb Exchange Terms in the RelativisticMean-Field Model with the Delta Meson and Isoscalar-Isovector Coupling," *Physical Review C,* vol. 104, p. 015804, 2021.

[6]   J. Zenihiro *et al*., "Neutron density distributions of 204,206,208Pb deduced via proton elastic scattering at Ep=295 MeV," *Physical Review C*, vol. 82, p. 044611, 2010.

[7]   S. Abrahamyan *et al*., "Measurement of the Neutron Radius of 208Pb through Parity Violation in Electron Scattering," *Physical Review Letter*, vol. 108, no. 11, p. 112502, 2012.

[8]   C. J. Horowitz *et al*., "Weak charge form factor and radius of 208Pb through parity violation in electron scattering," *Physical Review C*, vol. 85, p. 032501, 2012.

[9]   C. H. Hyun, "Neutron skin Thickness of 48Ca, 132Sn and 208Pb with KIDS density functional," arXiv: 2112, p. 00996, 2021.

[10]   R. Essick *et al*., "Astrophysical Constraint on the Symmetry Energy and the Neutron Skin of 208Pb with Minimal Modeling Assumptions," *Physical Review Letters*, vol. 127, no. 19, p. 192701, 2021.

[11]   N. Liliani *et al*., "Impacts of the tensor couplings of ω and ρ mesons and Coulomb-exchange terms on superheavy nuclei and their relation to the symmetry energy," *Physical Review C*, vol. 93, no. 5, p. 054322, 2016.

[12]   F. J. Fattoyev *et al*., "Neutron Skins and Neutron Stars in the Multimessenger Era," *Physical Review Letter*, vol. 120, p. 172702, 2018.

[13]   N. Liliani *et al*., "Pengaruh Kopling Tensor, Isovektor-Isoskalar Dan Pertukaran Elektromagnetik Terhadap Prediksi Double Magic Nuclei 292120," *Spektra: Jurnal Fisika dan Aplikasinya*, vol. 16, no. 1, pp. 28-33, 2015.

[14]   K. Zhang *et al*., "Nuclear Mass Table in Deformed Relativistic Hartree-Bogoliubov Theory in Continuum," Atomic Data and Nuclear Data Tables, vol. 144, p. 101488, 2022.

[15]   S. V. Pineda *et al*., "Charge Radius of Neutron-Deficient 54Ni and Symmetry Energy Constraints Using the Difference in Mirror Pair Charge Radii," *Physical Review Letter*, vol. 127, p. 182503, 2021.

[16]   T. G. Yue *et al*., "Constraints on the Symmetry Energy from PREX-II in the Multimessenger Era," *Physical Review Research*, vol. 4, no. 2, p. L022054, 2022.

[17]   B. T. Reed *et al*., "Implications of PREX-II on the equation of state of neutron-rich matter," *Physical Review Letter,* vol. 126, no. 17, p. 172503, 2021.